Analysis of radiative properties and direct radiative forcing estimates of dominant aerosol clusters over an urban-desert region in West Africa

Fawole, Olusegun G.; Cai, Xiaoming; Pinker, Rachel T.; Mackenzie, A. R.

DOI:
10.4209/aaqr.2017.12.0600
10.4209/aaqr.2017.12.0600

Document Version
Peer reviewed version

Citation for published version (Harvard):
Fawole, OG, Cai, X, Pinker, RT & Mackenzie, AR 2019, 'Analysis of radiative properties and direct radiative forcing estimates of dominant aerosol clusters over an urban-desert region in West Africa', *Aerosol and Air Quality Research*, vol. 19, no. 1, pp. 38-48. https://doi.org/10.4209/aaqr.2017.12.0600, https://doi.org/10.4209/aaqr.2017.12.0600

Analysis of radiative properties and direct radiative forcing estimates of dominant aerosol clusters over an urban-desert region in West Africa

Olusegun G. Fawole* [1, 2], Xiaoming Cai [2], Rachel T. Pinker [4], A.R. MacKenzie [2, 3]

[1] Department of Physics and Engineering Physics, Obafemi Awolowo University, Ile-Ife, Nigeria 220005

[2] School of Geography, Earth and Environmental Sciences, University of Birmingham, B15 2TT, UK

[3] Birmingham Institute of Forest Research (BIFoR), University of Birmingham, B15 2TT, UK

[4] Department of Atmospheric and Oceanic Science, University of Maryland, College Park, College Park, Maryland, U.S.A

* Corresponding author: gofawole@oauife.edu.ng

Abstract

The strategic location of the AERONET site (Ilorin) makes it possible to obtain information on several aerosol types and their radiative effects. The strong reversal of wind direction occasioned by the movement of the ITCZ during the West Africa Monsoon (WAM) plays a major role in the variability of aerosol nature at this site. Aerosol optical depth (AOD) (675 nm) and Angstrom exponent (AE) (440-870 nm) with 1st and 99th percentile values of 0.08 and 2.16, and 0.11 and 1.47, respectively, confirms the highly varying nature of aerosol at this site. Direct radiative forcing (DRF) and radiative forcing efficiency (RFE) of aerosol as retrieved from the AERONET sun-photometer measurements are estimated using radiative transfer calculations for the period 2005-2009 and 2011-2015. The DRF and RFE of dominant aerosol classes - desert dust (DD), biomass burning (BB), urban (UB) and gas flaring (GF) - have been estimated. Median (±standard deviation) values of DRF at top-of-atmosphere (TOA) for the DD, BB, UB and GF aerosol classes are -27.5±13.2 Wm^{-2}, -27.1±8.3 Wm^{-2}, -11.5±13.2 Wm^{-2} and -9.6±8.0 Wm^{-2}, respectively. While that of RFE for DD, BB, UB and GF aerosol classes are -26.2±4.1 $Wm^{-2}\delta^{-1}$, -35.2±4.6 $Wm^{-2}\delta^{-1}$, -31.0±8.4 $Wm^{-2}\delta^{-1}$ and -37.0±10.3 $Wm^{-2}\delta^{-1}$, respectively. The DD aerosol class showed the largest DRF but the smallest RFE, arguably, due to the high SSA and asymmetry factor values for this aerosol type. Its smallest AOD notwithstanding, the GF class could cause more perturbation to the Earth-Atmosphere system in the sub-region both directly and indirectly possibly due to the presence of black carbon and other co-emitted aerosol and the ageing of the GF aerosols. This study presents the first estimate of DRF for aerosols of gas flaring origin and shows that its radiative potential can be of similar magnitude to biomass burning, and urban aerosol in West Africa.

1 Introduction

Atmospheric aerosols perturb the Earth's radiative energy balance both indirectly and directly on regional and global scales (Charlson et al., 1992; Haywood and Shine, 1995; Rana et al., 2009). The ability of the aerosols to alter the amount of radiation depends on their concentration, composition, and particle size distribution (Verma et al., 2017). All of these determining factors vary significantly with aerosol sources. Increased concentrations of anthropogenic aerosols in the atmosphere since the pre-industrial times has been suggested to be partly responsible for the onset of global warming (IPCC, 2013).

When perturbation of the radiative budget of the Earth-atmosphere system results from the scattering and absorption of incoming solar radiation by atmospheric aerosol, the resulting radiative forcing is termed Direct Radiative Forcing (DRF). When atmospheric aerosols absorb radiation, they eventually dissipate such radiation, thereby altering the microphysical properties and lifetime of clouds, which invariably affect precipitation. Forcing resulting from such alterations is termed Indirect Radiative Forcing (IPCC, 2013). The contribution of aerosol to the total forcing due to well-mixed greenhouse gases is still associated with large uncertainties (Myhre, 2013).

The West African climate has a unique weather pattern due to the West African Monsoon (WAM) which is characterised by large-scale seasonal reversals of wind regimes (Sultan and Janicot, 2000; Barry and Chorley, 2009). The movement of the Intertropical Convergence Zone (ITCZ) and Intertropical front (ITF) are responsible for the seasonal reversal of the prevailing wind pattern in the region. Deep convection occurs in organised systems referred to as Mesoscale Convective System (MCS) (Mathon and Laurent, 2001). MCS associated with the ITCZ can lead to rapid uplift and large scale redistribution of aerosols (Reeves et al., 2010).

In recent years, in the West Africa region, anthropogenic emissions of aerosols and gaseous pollutants have increased substantially, largely due to increasing population and industrialisation; a trend expected to continue until 2030 (Liousse et al., 2014). Dominant anthropogenic sources of aerosol at the study site are fossil fuel combustion, vehicular emission, biomass burning, and industrial emission while the dominant natural aerosol source is desert dust. Despite growing evidences in support of the impacts of anthropogenic aerosols on regional radiative budget, strict regulations on emissions are still not available in major African cities and, where they are available, they are very weak (Liousse et al., 2012).

In Nigeria, the various wind patterns and seasons are associated with different dominant aerosol types. While the North-easterly Harmattan (NEH) wind, pre-dominant in the dry season (November- February), brings desert dust and biomass burning aerosols into the region. The South-westerly Monsoon (SWM) wind, associated with the onset of the WAM (April-October), brings predominantly urban and industrial aerosol which are believed to contain more carbonaceous aerosols (Knippertz et al., 2015). The properties and concentrations of these aerosol types vary significantly with the wind pattern. Studies of atmospheric aerosol and their radiative effects are very scarce in Nigeria.

In this study, the radiative properties of key aerosol types at this urban-desert station were analysed and their DRF and RFE at the TOA was estimated to provide the first estimate of climate forcing of gas-flaring aerosols in the region.

2 Methodology

2.1 Description of the AERONET site and prevailing climatic condition

The Ilorin AERONET site (8.32^{o} N, 4.34^{o} E) is located at a site between the densely populated monsoonal forest region of the south and Sahel Savannah region of the north. There is pronounced variation in the climatic conditions of the region governed by the movement of the intertropical convergence zone (ITCZ) and intertropical front (ITF), which

are responsible for the seasonal reversal of the wind direction (the West African Monsoon (WAM)).

The WAM is a coupled atmosphere-ocean-land system which is characterised by summer rainfall and winter drought (Lafore et al., 2010). The rainfall in the West African sub-region results essentially from the northward movement of the low-level monsoon airflow from March to August and the southward retreat from September to November. At their northern-most position, the humid monsoonal wind from the south meet driers and warmer air to form the ITF (Cornforth, 2012). During the dry season (November - March), the West Africa sub-region experiences strong emissions of pollutants resulting from extensive biomass burning of vegetation often from land preparation for the incoming planting season. During the wet season (May to October), the region is strongly influenced by mesoscale convective systems (MCS), which affects the compositions of the atmosphere through several ways including rapid vertical transport of aerosols to the upper troposphere (Law et al., 2010; Mari et al., 2011).

Gas flaring is a prominent and persistent source of atmospheric aerosols which includes soot (black carbon), SO_2, CO, NO_X (NO + NO_2), PAH and VOCs, especially in the oil-rich regions of the world (Fawole et al., 2016a). There are over 300 active flare sites in the region where an estimated 23.7 (44.4 metric tons of CO_2 equivalent) and 15.1 (28.3 metric ton of CO_2 equivalent) billion cubic meters (bcm) of natural gas is flared in 2006 and 2008, respectively (Elvidge et al., 2011; Fawole et al., 2016a). In 2012, of the 325 active flare sites identified in the Nigeria oil field, 97 (~ 30 %) ranked among the top 1000 largest flares out of the 7467 identified globally (Elvidge et al., 2015).

2.2 Trajectory calculation and classification

Seven-day (168 hours) back trajectories were calculated using the UK's Universities Global Atmospheric Modelling Programme (UGAMP) offline trajectory model. The model is driven by six-hourly ERA-Interim (European Centre for Medium-Range Weather Forecasts Interim Re-Analysis) wind analyses data. The trajectories of particles are calculated backward in time by interpolating these wind analysis to the current particle position. The position (latitude, longitude) and pressure were output every trajectory time step of 0.6 hours. The choice of 7-day back trajectory length is due to the atmospheric lifetime of between 5 and 9 days estimated for black carbon (BC) and particulate organic matter (POM), respectively (Cooke and Wilson, 1996; Cooke et al., 1997; Stier et al., 2006; Koch et al., 2009). Both BC and POM are major constituent of aerosol in the study area.

As shown in several studies, for example, Bibi et al. (2016) and Alam et al. (2016), atmospheric aerosols could be clustered using the inter-relationships between different pairs of their microphysical and optical properties. Using similar techniques, prominent aerosol classes were identified at the study site in Fawole et al. (2016b) as: Biomass burning (BB), Desert dust (DD), Urban (UB) and Gas flaring (GF) aerosols. In terms of optical and microphysical properties, these classes vary significantly (Fawole et al., 2016b); mixed classes (DD-BB, DD-UB, GF-UB and GF-DD) were also identified. Using similar clustering technique of analysing aerosol optical and microphysical properties, Bibi et al. (2016) classified aerosol in the Indo-Gangetic plains into dust, biomass and urban/industrial aerosol classes.

In this study, the properties of the single-source dominant classes was analysed to estimate their direct radiative forcing and forcing efficiency. For details of the trajectory classification and analysis of the variation of the optical and microphysical properties of the identified aerosol classes see Fawole et al. (2016b).

2.3 AERONET data analysis

The absolute magnitude of aerosol radiative forcing is determined, predominantly, by the values of aerosol optical depth (AOD) and single scattering albedo (SSA), while its sign is dependent on the SSA and surface albedo. Both AOD and SSA vary significantly with the source of the aerosol (Pani et al., 2016). In this study, Version 3 Level 1.5 of AERONET data released in January 2018 to which improved cloud screening and new quality controls have been applied were used to estimate the DRF and RFE of anthropogenic and natural aerosol classes in the West Africa sub-region. Adequate knowledge of aerosol SSA, hemispheric backscatter fraction (b) and AOD can be used to calculate the mean TOA aerosol radiative forcing for optically thin, partially absorbing aerosol (Haywood and Shine, 1995). For sites like Ilorin, where differences in the diurnal variation of aerosol properties (extensive and intensive) could be highly pronounced, the use of monthly averages of aerosol parameters will only provide highly generalised estimates of the optical and microphysical properties of the aerosol at such a site.

One of the key properties that determine the climate forcing ability of an aerosol is the angular distribution of the light scattered by the aerosol particles (Marshall et al., 1995). The angular distribution of scattered light intensity at a specific wavelength is referred to as the phase function (P). The asymmetry parameter, g, an important intensive parameter of aerosols for estimating its climate forcing ability could be derived from P. Values of g range between -1 for entirely backscattered light to +1 for entirely forward scattered light (Andrews et al., 2006). The fraction of backscattered light is the ratio of the integral of the volume scattering function over the backward half solid angle divided by the integral of the volume scattered function over the full solid angle (Horvath et al., 2016).

For AERONET retrievals, uncertainties in the direct sun measurements are within ± 0.01 for longer wavelengths greater than 440 nm and ± 0.02 for shorter wavelengths less than 440nm. AOD estimated uncertainty varies spectrally from ±0.01 to ±0.02 with the highest error in the ultraviolet wavelengths (Holben et al., 1998; Eck et al., 1999). For all sky radiance wavelengths (that is, 440, 675, 870, and 1020 nm), the uncertainty in SSA is expected to be ±0.03 based on Version 1almucantar retrieval computations (Dubovik et al., 2000; Holben et al., 2006).

2.3.1 Relationship between the asymmetry parameter and the backscatter fraction

Several studies (e.g., (Wiscombe and Grams (1976); Marshall et al. (1995); Kokhanovsky and Zege (1997))) have attempted to parameterise the backscatter fraction (b) in terms of the asymmetry parameter (g). Studies estimating aerosol DRF have either adopted an approximate relation between b and g or look-up tables of parameterisation of aerosol optical properties such as those of Hess et al. (1998) and D'Almeida et al. (1991).

In this study, assuming spherical particles, approximate relations given in equation (1) as cited in Horvath et al. (2016) and equation (2) according to Delene and Ogren (2002) have been used to estimate backscatter fraction (b) and average upscatter fraction, β , respectively.

$$b = \left[1.1\left(\frac{1}{1-g}\right)^{1.85} + 1\right]^{-1} \quad \text{.....(1)}$$

$$\beta = 0.0817 + 1.8495b + 2.9682b^2 \quad \text{.....(2)}$$

2.4 Aerosol Radiative Forcing

2.4.1 Estimating direct radiative forcing

The direct radiative forcing (DRF), ΔF, of aerosol at the top of the atmosphere (TOA) is estimated using the expression derived by Charlson et al. (1992). According to Haywood and

Shine (1995) the radiative transfer equation proposed by (Charlson et al. (1992)) is simplified as given in equation (3).

$$\Delta F \approx -DS_o{T_{at}}^2(1-A_c)\omega\overline{\beta}\bar{\delta}\times\left((1-R_s)^2-\frac{2R_s}{\overline{\beta}}\left(\frac{1}{\omega}-1\right)\right) \quad \text{..... (3)}$$

where D is the fractional day length, ω is the spectrally weighted single scattering albedo, S_o is the Solar constant, T_{at} is the atmospheric transmission, A_c is the fractional cloud amount, R_s is the surface reflectance, $\overline{\beta}$ is the spectrally weighted backscattered fraction and, $\bar{\delta}$ is the spectrally weighted AOD. The critical value of SSA at which the DRF shifts from positive to negative is dependent on the surface albedo and asymmetric parameter, g (Haywood and Boucher, 2000; Kassianov et al., 2007). One advantage of the analytical solution for the radiative transfer equation as stated above (equation (3)) over a radiative transfer model is an explicit dependence on individual parameters determining the radiative forcing (Chylek and Wong, 1995). As cloud cover (A_c) is a parameter in equation (3), to use the expression, the assumption is that the cloud cover is above the aerosol layer which is a typical atmospheric condition in the region considered in this study.

Schemes of wavelength-dependent aerosol parameters are time-consuming and quite complex to be incorporated into radiative forcing calculations and radiative transfer codes that can produce representative and accurate estimates of radiative forcing with one or two wavelength regions (Blanchet, 1982). In their study to examine the possibility of replacing aerosol parameters by wavelength-independent parameters and the accuracy and representativeness of such average parameters for the complete solar spectrum, Blanchet (1982) found out that results of calculations with average parameter are in close agreement with corresponding terms at a wavelength (λ) of 700 nm. Haywood (1995), using detailed radiative transfer codes, tested the representativeness of average aerosol parameter and found that results at around λ=700 nm were quite similar to those of using the entire solar spectrum.

215 Hence, the use of aerosol parameters at λ=675 nm, which is the nearest to 700 nm in the
216 range of wavelengths at which aerosol parameters are measured by AERONET sun-
217 photometers, in our estimations.

218 Fractional day-length, solar constant and atmospheric transmittance are assumed to be 0.5,
219 1370 W m^{-2} and 0.76, respectively (Haywood and Shine, 1995). To estimate DRF and RFE
220 of the different aerosol classes identified in Fawole et al. (2016b), monthly mean values of
221 cloud amount (A_c) was obtained from the ASOS-AWOS-METAR dataset (NOAA, 1998;
222 Yang et al., 2016) for the nearest airport (Cotonou) to the site, where sufficient amount of
223 cloud cover data are available. The surface reflectance data used are model output for albedo
224 simulations for Ilorin (2005 – 2009) (R.T Pinker, personal communication, August 2016).
225 Figure 1 presents the time series for the mean monthly surface albedo for Ilorin during 2005
226 – 2009. The yearly pattern of the variation of surface albedo (reflectance) is quite similar for
227 the five-year period model output available.
228

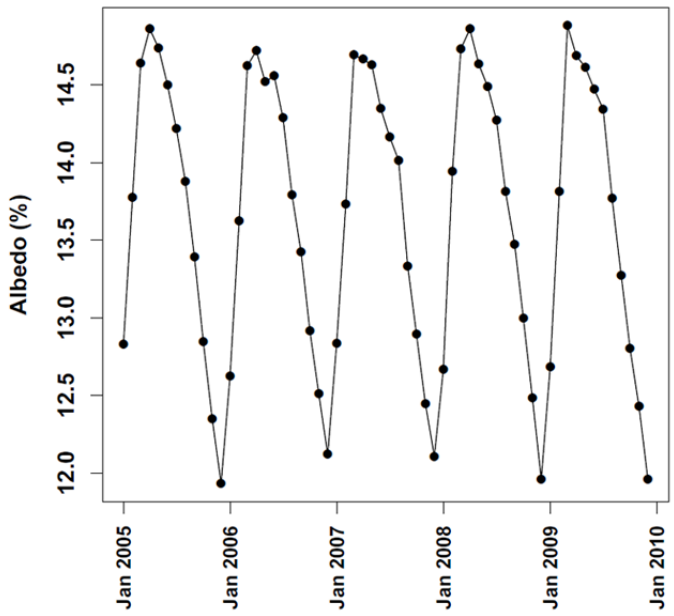

229

230 **Figure 1**: Time series for monthly mean surface albedo at Ilorin for the period (01/2005 –
231 12/2009).

2.4.2 Radiative forcing efficiency

SSA and backscatter fraction of the particle can be used to calculate the TOA aerosol forcing (ΔF) per unit aerosol optical depth (AOD); this is called aerosol forcing efficiency (Sheridan et al., 2002; Kaufman et al., 2005). In this study, to compare the forcing potential of the various aerosol classes, we estimated the forcing efficiency using equation (4). Forcing efficiency, ($^{\Delta F}/_{\delta}$), is the aerosol radiative forcing per unit AOD. AOD is a major extensive property of the aerosol, which determines the magnitude of its radiative forcing. Forcing efficiency depend only on the nature and composition of the aerosol rather than its amount (Sheridan and Ogren, 1999).

$$\frac{\Delta F}{\delta} = -DS_o{T_{at}}^2(1-A_c)\omega\overline{\beta} \times \left((1-R_s)^2 - \frac{2R_s}{\overline{\beta}}\left(\frac{1}{\omega}-1\right)\right) \quad \text{..... (4)}$$

Virkkula et al. (2014), in their study to assess the effect of aerosol from different phases of biomass burning - flaming and smouldering - on the chemical and physical properties of airborne aerosols in the Boreal forest, used the expression in equation (4) to estimate the radiative forcing efficiency of the biomass burning aerosols. Rizzo et al. (2013), using equation (4), estimated aerosol forcing efficiency over a primary forest site in Amazonia.

3 Results and discussions

3.1 Climatology of aerosol properties

Significant variation of aerosol optical and microphysical properties in the multiyear analysis of aerosol properties at the Ilorin AERONET site is a strong indication of the varying sources of aerosols at the site. The range of values, at λ=675 nm, for aerosol optical depth (AOD), single scattering albedo (SSA) and asymmetry parameter (*g*) are 0.04 – 3.71, 0.68 – 0.99, and 0.58 – 0.8, respectively. The variation of aerosol properties is more pronounced between the non-WAM and WAM months due to seasonal reversal of the prevailing wind direction, and hence, a change of dominant sources of aerosols.

3.1.1 Temporal variability of Aerosol Optical Depth, Fine Mode Fraction and Angström exponent

During the NEH months (November - February), the values of the aerosol optical depth (AOD_{675}) and Angström Exponent ($AE_{440-870}$) are 1.22±0.17 and 0.35±0.06, respectively. These are months of intense biomass burning in the West African sub-region as well as intrusion of dust from the Sahara and Sahel regions. Aerosol loading in the SWM months (April - October), are characterised by lower AOD (675 nm) and high AE (440-870 nm) with median values of 0.58±0.23 and 1.02±0.19, respectively (see Figure 2). The monthly plots in Figure 2 are obtained from average daily data of aerosol parameters. Compared to AE values for similar dust sites, the relatively high average AE value of the dust aerosol in the NEH months is probably due to contributions of biomass burning aerosol at that time of the year (Fawole et al., 2016b).

The significant seasonal pattern in the AE and fine mode fraction (FMF) of aerosol at the site, as seen in Figure 2(b) and 2(c), is due to varying aerosol sources and/or changes in atmospheric transport. There is the dominance of fine mode aerosol fraction during the West Africa Monsoon months when the prevailing wind is the moist SWM. The influx of urban-industrial air is expected to predominate during the WAM months, between April and October (Fawole et al., 2016b). The value of AE peaks between July and September and is lowest between February and March. The lower AE values during the peak of the dry season show the strong intrusion of dust in this region at that period of the year. During the WAM months, the peak AE values between July and September coincide with the peak values of backscatter fraction, *b* (see Figures 2(b) and 3(b)). This strongly suggests an increase in fine particle fraction, which is attributable to inflow of urban and industrial emissions from the south of the AERONET site. The variation of aerosol parameter with prevailing Monsoonal wind as observed in this study has been observed in similar studies over Karachi, Pakistan

during the period 2006-2008 (Bibi et al., 2017) and Ahmedabad, India (Ramachandran and Kedia, 2010).

3.1.2 Temporal variability of single scattering albedo (SSA) and backscatter fraction

In the West Africa sub-region, there are significant differences in the relative amount of scattering and absorption of aerosols at different periods of the year. These differences result in the variation of SSA during the years as shown Figures 3(a). During the SWM months, as shown in the multiyear mean monthly SSA values in Figures 3(a), inland flow of south-westerly monsoon winds are rich in partially absorbing aerosols from the urban and industrial site including gas flaring emissions from the intense gas flaring activities in the Niger Delta region. In Figure 3(a), the WAM months (April –August) exhibit the widest range of SSA (0.66-0.98) which could result in a wider range of DRF. This wide range of SSA could be attributable to the diverse nature of aerosol in the urban and industrial emissions from the south of Ilorin.

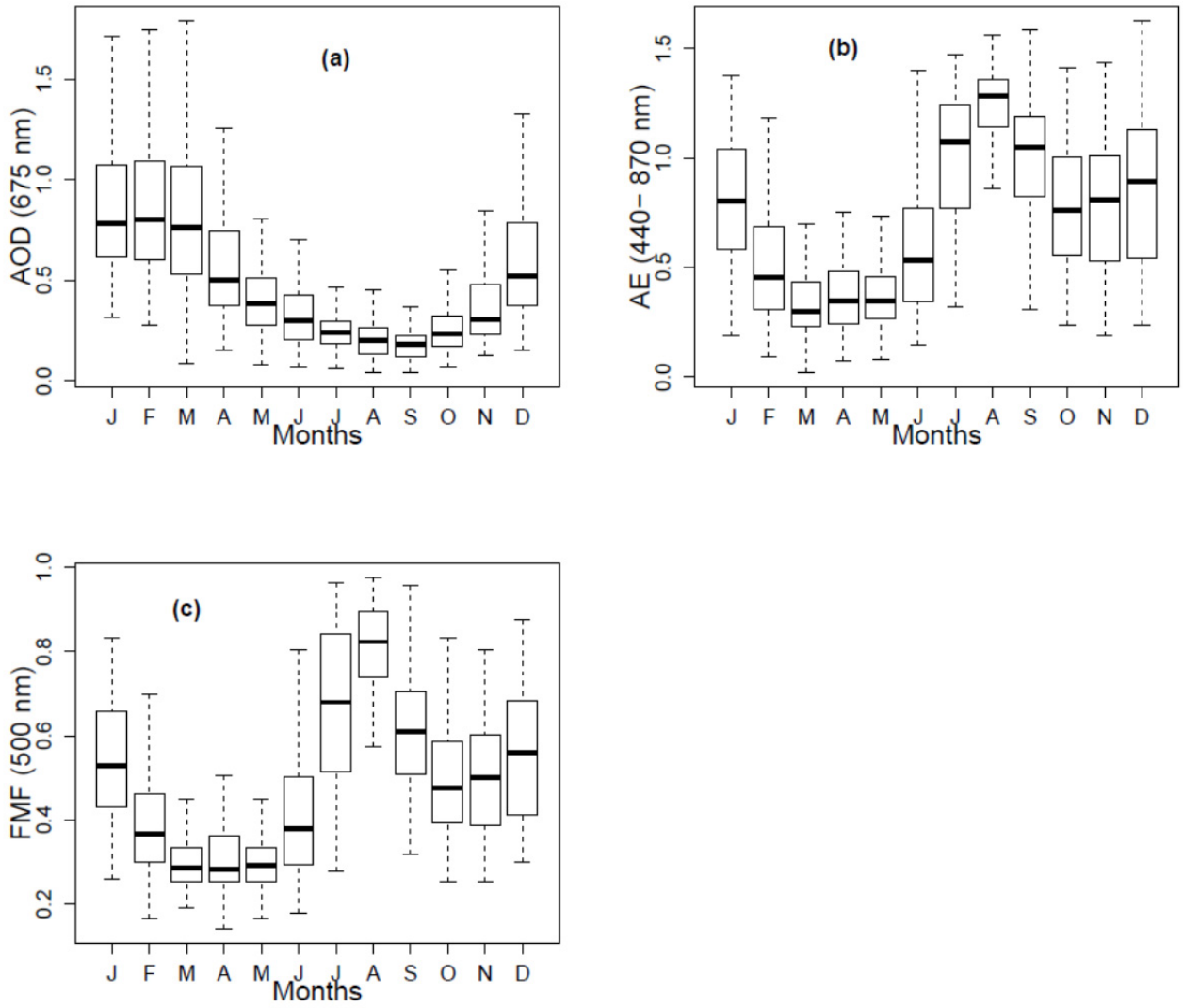

296
297 **Figure 2**: Multiyear monthly variations of (a) AOD, (b) Angstrom exponent (AE), and (c)
298 Fine Mode Fraction (FMF) of aerosol during the year 2005-2015
299

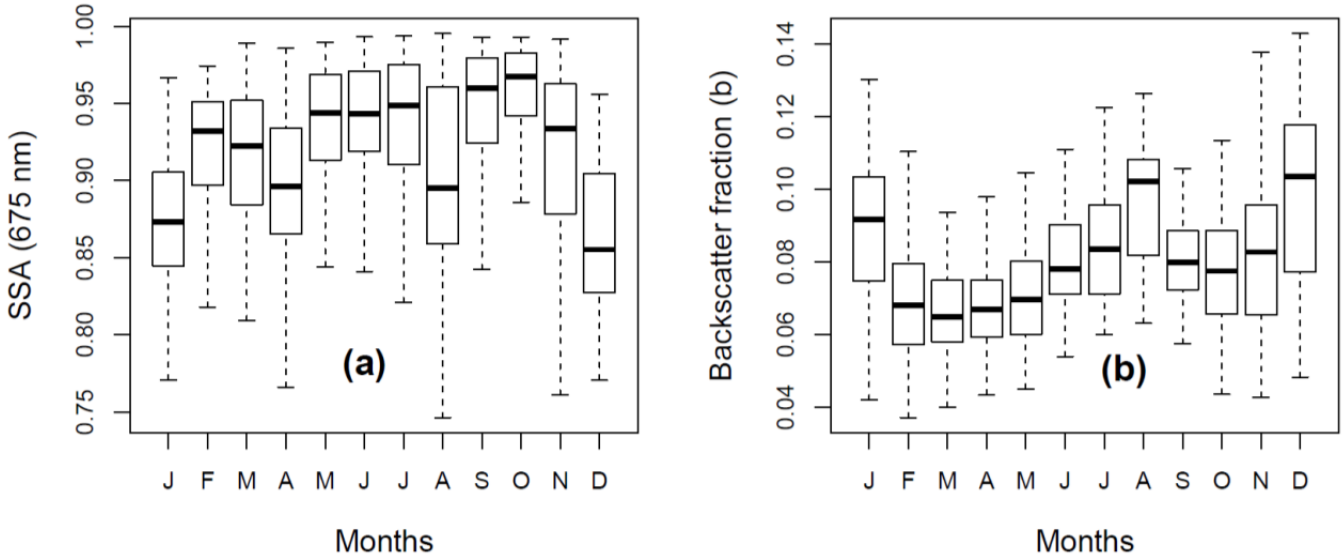

300
301 **Figure 3**: Multiyear average monthly (a) variation of SSA (675 nm) and (b) variation of
302 backscatter fraction during the year 2005-2015

The boxplots in Figure 3(b) show a steady increase in the backscatter fraction from the lowest average values of 0.07±0.01 during March (peak of the NEH months) to the highest average values of 0.1±0.02 during the peak of the WAM months. The median values of the backscatter fraction of the non-WAM and WAM months correspond to asymmetric parameter (*g*) values of 0.72±0.1 and 0.61±0.1, respectively. This arguably suggests a steady increase in the concentration of fine-mode aerosol fraction during the WAM months which is attributable to increased inflow of combustion aerosols from urban and industrial emissions. Mie theory predicts a higher backscatter fraction for fine-mode spherical aerosol particles (Andrews et al., 2011). The wide range of backscatter fraction during the non-WAM months (NDJF) is due to mixture of biomass burning and intrusion of desert dust which are intense during the Harmattan haze period in the region. The mean monthly value of backscatter fraction in Figure 3(b) shows a bi-modal distribution with peaks during the intense biomass burning season (NDJ) and the peak of the WAM months (July-August) when the ITCZ is northernmost allowing enhanced inland flow of aerosol from south of the AERONET site.

3.2 Variability of Angström exponent and (AOD) for the aerosol classes

The median (±standard deviation) values of the optical and microphysical properties of the identified aerosol classes are presented in Table 1. Unless otherwise stated, average values of aerosol parameters are reported at 675 nm. The Angström exponents (AE) discussed for the aerosol classes were estimated using the 440 nm and 870 nm wavelength pair. The highly varying range of AOD_{440} and AE values; 0.07 – 3.87 and 0.01 – 1.74, respectively, strongly suggests a broad range of contributing sources to the aerosol loading at the study site. As the distribution of most of the aerosol parameters for the classes are non-Gaussian, the median values are reported with the standard deviations given in brackets.

3.2.1 Desert dust (DD)

The DD aerosol class consists of 209 days of aerosol signals, which are predominant in the NEH months and the early days of the onset of WAM months. The major source of desert dust considered in this class classification is the Sahara and Sahel dust regions (13 – 18^{o} N; 6 – 17^{o} E). The median values of AOD_{440} and $AE_{440\text{-}870}$ for this aerosol class is 1.13(±0.54) and 0.3(±0.12), respectively. These values agree well with those from studies for similar sites in the Bodélé depression of Northern Chad (Todd et al., 2007), Indo-Gangetic plains (Bibi et al., 2016) and dust regions of China (Wang et al., 2004). The average value for AOD is highest for the desert dust class while AE is the least. With a median SSA value of 0.95(±0.02), this class is the least absorbing.

3.2.2 Urban aerosol (UB)

Aerosol signature in the urban aerosol class is prominent in the WAM months when the south-westerly moist monsoon wind is prevalent in the region. For this class, the median AOD_{440} and AE values are 0.53(±0.35) and 0.52(±0.34), respectively. Even though this AE value is low, it is still higher than that for the DD aerosol class. The DD aerosol class is expected to contain a higher fraction of coarse aerosol. This class of aerosol (Urban), with a median value of SSA of 0.93(±0.04), is partially absorbing arguably due to increased carbonaceous particle content from anthropogenic sources in the urban area.

3.2.3 Gas flaring aerosol (GF)

This class is similar to the urban class but has a lower median value of AOD_{440} and an average AE value, which is higher than that of the urban aerosol by a factor of ~2. For this class, the median values of AOD_{440} and AE values are 0.41(±0.26) and 1.16(±0.29), respectively. A median value of SSA of 0.9(0.06) makes it more absorbing than the urban aerosol class, which is attributable to it having a relatively higher carbonaceous particulate

content. This class is estimated to have an average Absorption Angstrom Exponent (AAE) of 0.98(±0.25) in contrast to urban aerosols, which has an AAE value of 1.2(±0.38) (Fawole et al., 2016b). The gas-flaring region, south of the AERONET site, contains more than 300 active flares (Elvidge et al., 2015), where it is estimated that more than 25 % of the annual natural gas production is flared (Elvidge et al., 2009; Ite and Ibok, 2013; Anejionu et al., 2015).

It should, however, be noted that gas flaring, a prominent source of soot (BC), also emit other aerosol including volatile organic compounds (VOCs), SO_2 and NO_X, some of which exert a cooling effect on the climate (USEPA, 2012).

3.2.4 Biomass burning

Similar to findings from the studies by Bibi et al. (2016) and (Tiwari et al., 2016), the BB aerosol class is characterised by high AOD and high AE, which is typical of biomass burning sites. Although, it is prevalent almost at the same time as the desert dust season during the NEH months, it can be distinguish by its lower SSA and higher AE values. For this class, the median values of AOD_{440} and AE are 0.93(±0.3) and 1.0(±0.25), respectively. The range of values for AOD_{440} and AE are in agreement with values reported by Ogunjobi et al. (2008) and (Pace et al., 2006) for similar biomass burning sites in West Africa and around Central Mediterranean, respectively. The region of biomass burning considered in the classification of this class are (i) 6.5 – 11.5^o N; 3^o W – 3^o E and (ii) 6.5 – 11.5^o N; 13.6^o E – 22.5^o E (see Fawole et al. (2016b)). The choice of these BB regions are based on data obtained from MODIS active fire detection over Africa as reported by Roberts et al. (2009). In agreement with reports from previous studies from similar sites, this class, with median SSA value of 0.86 (±0.04), is the most absorbing class presumably due to its enhanced organic carbon (OC) content.

Table 2 presents the mean monthly surface reflectance, R_S, and cloud amount, A_C used in the DRF estimation. Sources of these parameters are stated in section 2.4.1.

Table 1: Summary of parameter for aerosol classes used to estimate their DRF

	Backscatter fraction (b)	AOD (675 nm)	Asymmetry parameter (675 nm)	SSA (675 nm)	DRF (Wm^{-2})	Forcing efficiency (FE) ($Wm^{-2}\delta^{-1}$)
DD	**0.06±0.01**	**0.91±0.44**	**0.74±0.03**	**0.97±0.02**	**-30.3±13.4**	**-31.0±3.3**
BB	**0.1±0.02**	**0.61±0.26**	**0.66±0.03**	**0.87±0.03**	**-23.6±8.9**	**-39.0±4.0**
UB	**0.08±0.02**	**0.38±0.23**	**0.70±0.03**	**0.96±0.04**	**-11.7±7.5**	**-32.4±5.4**
GF	**0.1±0.02**	**0.29±0.21**	**0.66±0.04**	**0.91±0.06**	**-8.2±5.8**	**-36.0±7.8**

Table 2: Mean monthly surface reflectance and cloud amount for study site

	Jan	Feb	Mar	Apr	May	Jun	Jul	Aug	Sept	Oct	Nov	Dec
R_s	**0.13**	**0.14**	**0.15**	**0.15**	**0.15**	**0.14**	**0.14**	**0.14**	**0.13**	**0.13**	**0.12**	**0.12**
Cloud amount	**0.22**	**0.35**	**0.35**	**0.35**	**0.35**	**0.35**	**0.35**	**0.35**	**0.35**	**0.35**	**0.35**	**0.15**

3.3 Aerosol radiative forcing

The direct radiative forcing (DRF) for each aerosol class at the TOA was estimated using the relationship in equation (3). The values of surface reflectance, R_s, and cloud amount, A_C used in the estimations range between 0.12 – 0.15 and 0.15 – 0.39, respectively. Table 1 presents, for each cluster, the range of values of AOD (τ), SSA (ω), backscatter fraction (b) used in the DRF estimations. The daily average values of these aerosol parameters were used for the DRF estimations of the four classes.

Figure 4 presents the variation of the DRF estimates at TOA for each aerosol cluster. The DD aerosol class with median AOD_{675} value of 0.91(±0.44) has the highest DRF of -30.3±13.4

392 Wm^{-2} at TOA. Of the four classes identified, this class has the highest mean AOD. The
393 median DRF value for this class, as shown in Figure 4, is highest. It is believed that this high
394 DRF value is due to the large SSA (average value of 0.97±0.02), which brings about less
395 absorption and more scattering, and the largest asymmetry factor, *g*, of 0.74±0.03, which
396 causes more forward scattering of incoming radiation, compared to the other aerosol classes.
397 Thus, consistent with the findings of García et al. (2012), this class has the most effective
398 cooling effect on the earth-atmosphere system at the TOA in the region.

399 The biomass burning (BB) aerosols class has an estimated DRF of -23.6±8.9 Wm^{-2} at TOA
400 with average AOD_{675} value of 0.61(±0.26). Compared to the DD class, this class has a
401 relatively shorter range of DRF. This value of DRF is comparable to the mean DRF obtained
402 by García et al. (2012) and Yoon et al. (2005) for similar biomass burning site in South
403 America and South Africa, respectively. Compared to the DD and BB aerosol classes, the
404 urban (UB) class exerts a smaller cooling effect. This class (urban) with average AOD_{675} of
405 0.38(±0.23), rich in anthropogenic urban aerosol is estimated to have a DRF value of -
406 11.7(±7.5) Wm^{-2}. In a study by Yoon et al. (2005), similar values of DRF was obtained for
407 US East Coast (Goddard Space Flight Center (GSFC)), a heavily populated urban area. With
408 median DRF value of -8.2±5.8 Wm^{-2} (AOD_{675} = 0.29±0.21), the GF class has the least
409 cooling effect at TOA. The GF class is believe to be rich in fossil fuel combustion emissions
410 including sulfate and black carbon (Fawole et al., 2016a)

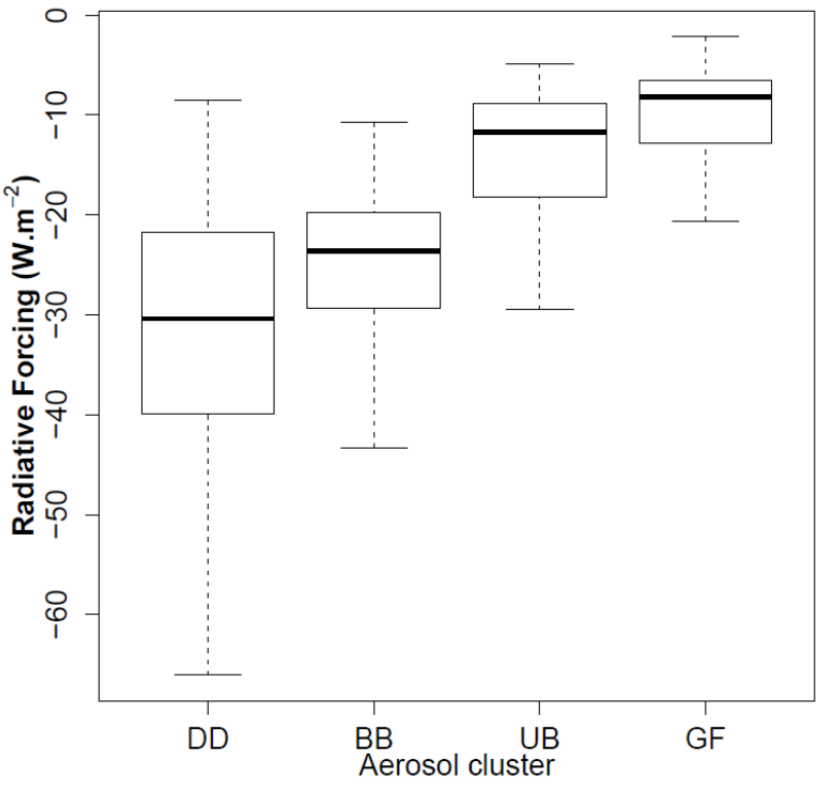

411
412 **Figure 4**: Direct radiative forcing (DRF) at the TOA for the different aerosol classes

413

414 **3.4 Radiative forcing efficiency (RFE)**

415 The absolute magnitude of the DRF is dependent not only on the amount of radiation entering
416 the atmosphere but also on the quantity of aerosol perturbing the atmosphere (Bush and
417 Valero, 2003). For a better understanding of the impact of aerosol optical depth (AOD) on the
418 estimation of aerosol DRF, the radiative forcing efficiency (RFE) of the different classes was
419 estimated using equation (4). Since RFE is independent of AOD, it is a useful tool to compare
420 the forcing abilities of different aerosol types. As such, the influences of other variables, such
421 as SSA, absorption and scattering properties and, surface albedo might become more evident
422 (García et al., 2012).

423 Figure 5 shows the variation of the RFE for the different aerosol classes. The natural aerosol,
424 desert dust (DD), has the least average RFE of -31.0±3.3 $Wm^{-2}\delta^{-1}$. The BB aerosol class, like
425 the DD class, has a short range of RFE, but a higher mean RFE value of -39.0±4.0 $Wm^{-2}\delta^{-1}$.

The UB and GF aerosol classes have average RFE values of -32.4±5.4 and -36.0±7.8, respectively. The BB aerosol class has the highest median RFE value. These two classes (UB and GF), compared to the DD and BB aerosol classes, have relatively wider ranges of RFE. As such, aerosols in these two classes have the ability to perturb the Earth-atmosphere system more in this region.

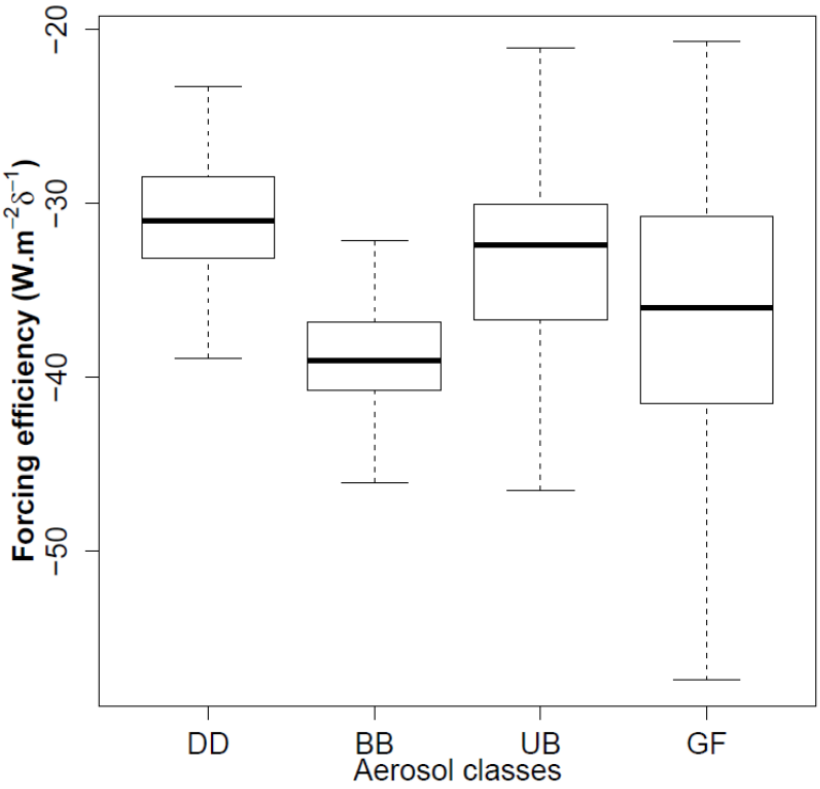

Figure 5: Radiative forcing efficiency (RFE) for the different classes

Figure 6 presents the relationship between DRF and aerosol optical depth AOD_{675} for the different aerosol types. The slope of best-fit line, shown in red, gives the average forcing efficiency, as estimated by equation (4). The regression equation for the plot and correlation of DRF and AOD values are also shown in red on Figure 6. In Figure 6, N is the number of days clustered into each aerosol class.

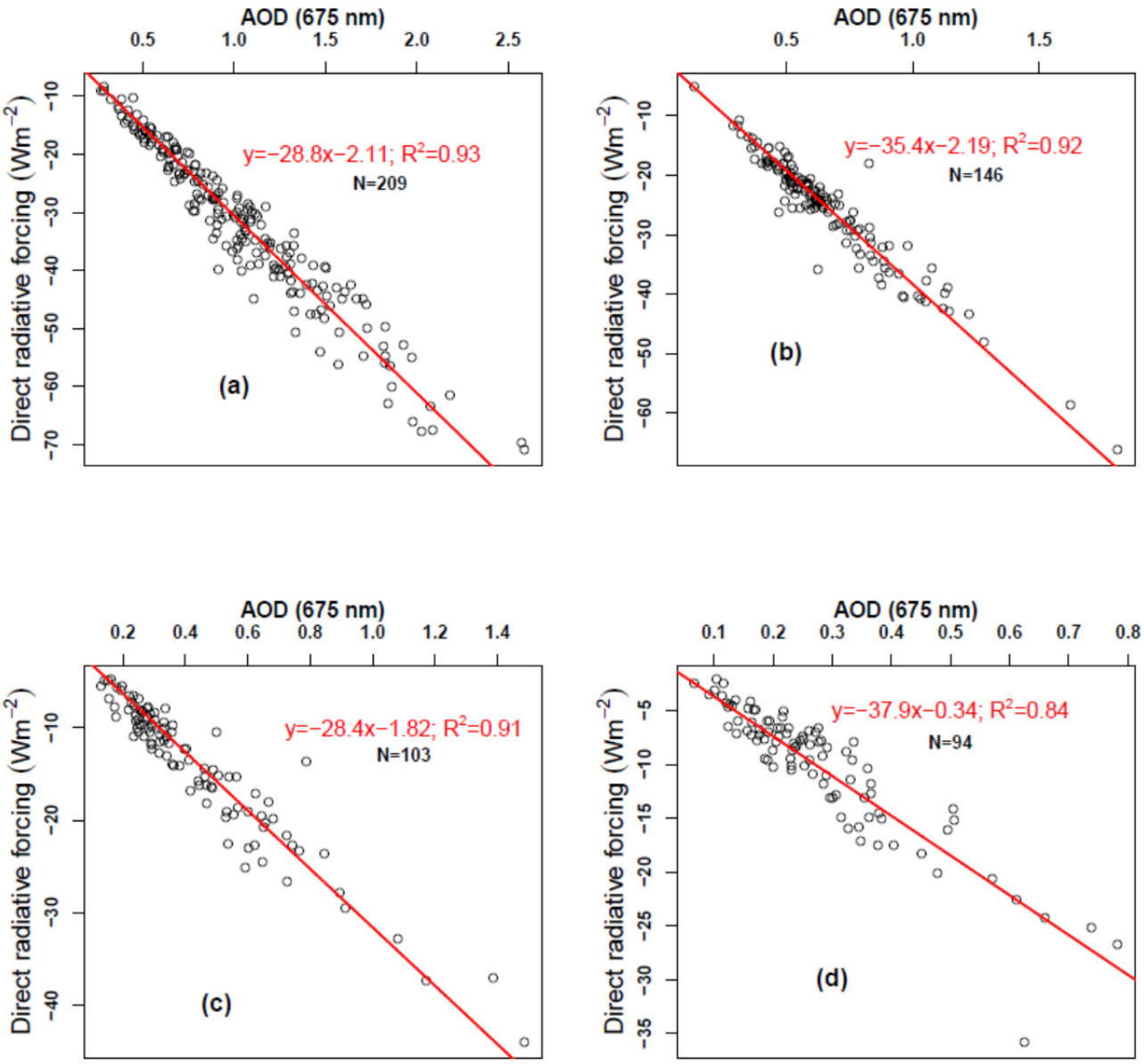

Figure 6: The relationship between DRF and AOD (675 nm) for (a) Desert dust cluster (b) Biomass burning cluster, (c) Urban cluster and (d) Gas flaring cluster.

4 Conclusion

The variations of the aerosol optical and microphysical parameters – AOD, SSA, asymmetric parameter, Angstrom exponent and backscatter fraction – were studied for the West African sub-region using AERONET retrievals from Ilorin, Nigeria. The DD aerosol class is characterised by high AOD and low AE. The BB aerosol class is characterised by high AOD and high AE while the GF class is characterised by low AOD and high AE. The direct radiative forcing of the various dominant aerosol types has been estimated using aerosol

parameters from AERONET retrievals as inputs in a simplified radiative transfer equation proposed by Haywood and Shine (1995). Due to differences in methodologies and varying aerosol sources/nature, it is difficult to directly compare results (average DRF values) from literature. Desert dust (DD) and biomass burning aerosols were found to be the most effective cooling aerosol at the TOA in the region. UB and GF aerosol classes which are suggested to be rich in emissions from the combustion of fossil fuel (i.e. black carbon and sulphate) have less cooling effects. The more absorbing aerosols (GF and BB) show the higher forcing efficiency; and, GF aerosol class, the largest variability in RFE. These results suggest the need for concerted efforts to adequately characterise and quantify emissions from real-world gas flares as they make significant contributions to the radiative transfer in the Earth-atmosphere system, particularly in oil-rich regions, where gas flaring is persistent, continuous and substantial. To the best of our knowledge, this is the first estimate of DRF for gas-flaring dominant aerosol class.

Findings from this study, especially as it relates to the GF cluster, suggest the need for an adequate understanding of the behaviour and transformation of atmospheric aerosol of gas flaring origin. A chemistry transport model with adequate schemes to simulate the behaviour of aerosols will be very appropriate for this proposed study.

5 References

Alam, K., Shaheen, K., Blaschke, T., Chishtie, F., Khan, H.U. and Haq, B.S. (2016). Classification of Aerosols in an Urban Environment on the Basis of Optical Measurements. *Aerosol and Air Quality Research* 16: 2535-2549.

Andrews, E., Ogren, J., Bonasoni, P., Marinoni, A., Cuevas, E., Rodríguez, S., Sun, J., Jaffe, D., Fischer, E. and Baltensperger, U. (2011). Climatology of Aerosol Radiative Properties in the Free Troposphere. *Atmospheric Research* 102: 365-393.

Andrews, E., Sheridan, P., Fiebig, M., McComiskey, A., Ogren, J., Arnott, P., Covert, D., Elleman, R., Gasparini, R. and Collins, D. (2006). Comparison of Methods for Deriving Aerosol Asymmetry Parameter. *Journal of Geophysical Research: Atmospheres* 111: D05S04, doi:10.1029/2004JD005734.

Anejionu, O.C., Blackburn, G.A. and Whyatt, J.D. (2015). Detecting Gas Flares and Estimating Flaring Volumes at Individual Flow Stations Using Modis Data. *Remote Sensing of Environment* 158: 81-94.

Barry, R.G. and Chorley, R.J. (2009). *Atmosphere, Weather and Climate*. Routledge.

Bibi, H., Alam, K. and Bibi, S. (2016). In-Depth Discrimination of Aerosol Types Using Multiple Clustering Techniques over Four Locations in Indo-Gangetic Plains. *Atmospheric Research* 181: 106-114.

Bibi, S., Alam, K., Chishtie, F., Bibi, H. and Rahman, S. (2017). Observations of Black Carbon Aerosols Characteristics over an Urban Environment: Radiative Forcing and Related Implications. *Science of the Total Environment* 603: 319-329.

Blanchet, J.P. (1982). Application of the Chandrasekhar Mean to Aerosol Optical Parameters. *Atmosphere-Ocean* 20: 189-206.

Bush, B.C. and Valero, F.P. (2003). Surface Aerosol Radiative Forcing at Gosan During the Ace-Asia Campaign. *Journal of Geophysical Research: Atmospheres* 108.

Charlson, R., Schwartz, S., Hales, J., Cess, R., Coakley, J., Hansen, J. and Hofmann, D. (1992). Climate Forcing by Anthropogenic Aerosols. *Science* 255: 423-430.

Chylek, P. and Wong, J. (1995). Effect of Absorbing Aerosols on Global Radiation Budget. *Geophysical Research Letters* 22: 929-931.

Cooke, W.F., Jennings, S. and Spain, T. (1997). Black Carbon Measurements at Mace Head, 1989–1996. *Journal of Geophysical Research: Atmospheres* 102: 25339-25346.

Cooke, W.F. and Wilson, J.J. (1996). A Global Black Carbon Aerosol Model. *Journal of Geophysical Research: Atmospheres* 101: 19395-19409.

Cornforth, R. (2012). Overview of the West African Monsoon 20111. *Weather* 67: 59-65.

D'Almeida, G.A., Koepke, P. and Shettle, E.P. (1991). *Atmospheric Aerosols: Global Climatology and Radiative Characteristics*. A Deepak Pub.

Delene, D.J. and Ogren, J.A. (2002). Variability of Aerosol Optical Properties at Four North American Surface Monitoring Sites. *Journal of the Atmospheric Sciences* 59: 1135-1150.

Dubovik, O., Smirnov, A., Holben, B., King, M., Kaufman, Y., Eck, T. and Slutsker, I. (2000). Accuracy Assessments of Aerosol Optical Properties Retrieved from Aerosol Robotic Network (Aeronet) Sun and Sky Radiance Measurements. *Journal of Geophysical Research: Atmospheres* 105: 9791-9806.

Eck, T., Holben, B., Reid, J., Dubovik, O., Smirnov, A., O'Neill, N., Slutsker, I. and Kinne, S. (1999). Wavelength Dependence of the Optical Depth of Biomass Burning, Urban, and Desert Dust Aerosols. *J Geophys Res* 104: 00093-00095.

Elvidge, C.D., Baugh, K.E., Ziskin, D., Anderson, S. and Ghosh, T. (2011). Estimation of Gas Flaring Volumes Using Nasa Modis Fire Detection Products. *NOAA National Geophysical Data Center (NGDC), annual report* 8.

Elvidge, C.D., Zhizhin, M., Baugh, K., Hsu, F.-C. and Ghosh, T. (2015). Methods for Global Survey of Natural Gas Flaring from Visible Infrared Imaging Radiometer Suite Data. *Energies* 9: 14.

Elvidge, C.D., Ziskin, D., Baugh, K.E., Tuttle, B.T., Ghosh, T., Pack, D.W., Erwin, E.H. and Zhizhin, M. (2009). A Fifteen Year Record of Global Natural Gas Flaring Derived from Satellite Data. *Energies* 2: 595-622.

Fawole, O., Cai, X.-M. and MacKenzie, A. (2016a). Gas Flaring and Resultant Air Pollution: A Review Focusing on Black Carbon. *Environmental Pollution* 216: 182-197. doi: 110.1016/j.envpol.2016.1005.1075.

Fawole, O.G., Cai, X., Levine, J.G., Pinker, R.T. and MacKenzie, A. (2016b). Detection of a Gas Flaring Signature in the Aeronet Optical Properties of Aerosols at a Tropical Station in West Africa. *Journal of Geophysical Research: Atmospheres* 121: 14513–14524.

García, O., Díaz, J., Expósito, F., Díaz, A., Dubovik, O., Dubuisson, P. and Roger, J.-C. (2012). Shortwave Radiative Forcing and Efficiency of Key Aerosol Types Using Aeronet Data. *Atmospheric Chemistry and Physics* 12: 5129.

Haywood, J. and Boucher, O. (2000). Estimates of the Direct and Indirect Radiative Forcing Due to Tropospheric Aerosols: A Review. *Reviews of geophysics* 38: 513-543.

Haywood, J. and Shine, K. (1995). The Effect of Anthropogenic Sulfate and Soot Aerosol on the Clear Sky Planetary Radiation Budget. *Geophysical Research Letters* 22: 603-606.

Haywood, J.M. (1995). Model Investigations into the Radiative Forcing of Climate by Anthropogenic Emissions of Sulphate and Soot Aerosol, University of Reading, United Kingdom, p. 247.

Hess, M., Koepke, P. and Schult, I. (1998). Optical Properties of Aerosols and Clouds: The Software Package Opac. *Bulletin of the American meteorological society* 79: 831-844.

Holben, B., Eck, T., Slutsker, I., Smirnov, A., Sinyuk, A., Schafer, J., Giles, D. and Dubovik, O. In (Ed.)^(Eds.) Asia-Pacific Remote Sensing Symposium, 2006, International Society for Optics and Photonics, pp. 64080Q-64080Q-64014.

Holben, B., Eck, T., Slutsker, I., Tanre, D., Buis, J., Setzer, A., Vermote, E., Reagan, J., Kaufman, Y. and Nakajima, T. (1998). Aeronet—a Federated Instrument Network and Data Archive for Aerosol Characterization. *Remote sensing of environment* 66: 1-16.

Horvath, H., Kasahara, M., Tohno, S., Olmo, F., Lyamani, H., Alados-Arboledas, L., Quirantes, A. and Cachorro, V. (2016). Relationship between Fraction of Backscattered Light and Asymmetry Parameter. *Journal of Aerosol Science* 91: 43-53.

IPCC (2013). *Climate Change 2013: The Physical Science Basis. Contribution of Working Group I to the Fifth Assessment Report of the Intergovernmental Panel on Climate Change [Stocker, T.F, D. Qin, G.K. Plattner, M. Tignor, S.K. Allen, J. Boschung, A. Nauels, Y. Xia, B. Bex, and B.M. Midgley (Eds)]*. Cambridge University Press, Cambridge, United Kingdom and New York, NY, USA.

Ite, A.E. and Ibok, U.J. (2013). Gas Flaring and Venting Associated with Petroleum Exploration and Production in the Nigeria's Niger Delta. *American Journal of Environmental Protection* 1: 70-77.

Kassianov, E.I., Flynn, C.J., Ackerman, T.P. and Barnard, J.C. (2007). Aerosol Single-Scattering Albedo and Asymmetry Parameter from Mfrsr Observations During the Arm Aerosol Iop 2003. *Atmospheric Chemistry and Physics* 7: 3341-3351.

Kaufman, Y., Koren, I., Remer, L., Tanré, D., Ginoux, P. and Fan, S. (2005). Dust Transport and Deposition Observed from the Terra-Moderate Resolution Imaging Spectroradiometer (Modis) Spacecraft over the Atlantic Ocean. *Journal of Geophysical Research: Atmospheres* 110.

Knippertz, P., Evans, M.J., Field, P.R., Fink, A.H., Liousse, C. and Marsham, J.H. (2015). The Possible Role of Local Air Pollution in Climate Change in West Africa. *Nature Climate Change* 5: 815-822.

Koch, D., Schulz, M., Kinne, S., McNaughton, C., Spackman, J., Balkanski, Y., Bauer, S., Berntsen, T., Bond, T.C. and Boucher, O. (2009). Evaluation of Black Carbon Estimations in Global Aerosol Models. *Atmospheric Chemistry and Physics* 9: 9001-9026.

Kokhanovsky, A. and Zege, E. (1997). Optical Properties of Aerosol Particles: A Review of Approximate Analytical Solutions. *Journal of aerosol science* 28: 1-21.

Lafore, J.P., Flamant, C., Giraud, V., Guichard, F., Knippertz, P., Mahfouf, J.F., Mascart, P. and Williams, E. (2010). Introduction to the Amma Special Issue on 'Advances in Understanding Atmospheric Processes

over West Africa through the Amma Field Campaign'. *Quarterly Journal of the Royal Meteorological Society* 136: 2-7.

Law, K.S., Fierli, F., Cairo, F., Schlager, H., Borrmann, S., Streibel, M., Real, E., Kunkel, D., Schiller, C. and Ravegnani, F. (2010). Air Mass Origins Influencing Ttl Chemical Composition over West Africa During 2006 Summer Monsoon. *Atmospheric Chemistry and Physics* 10: 10753-10770.

Liousse, C., Assamoi, E., Criqui, P., Granier, C. and Rosset, R. (2014). Explosive Growth in African Combustion Emissions from 2005 to 2030. *Environmental Research Letters* 9: 035003.

Liousse, C., Galy-Lacaux, C., Ndiaye, S.A., Diop, B., Ouafo, M., Assamoi, E.M., Gardrat, E., Castera, P., Rosset, R. and Akpo, A. (2012). Real Time Black Carbon Measurements in West and Central Africa Urban Sites. *Atmospheric environment* 54: 529-537.

Mari, C.H., Reeves, C.E., Law, K.S., Ancellet, G., Andrés-Hernández, M.D., Barret, B., Bechara, J., Borbon, A., Bouarar, I. and Cairo, F. (2011). Atmospheric Composition of West Africa: Highlights from the Amma International Program. *Atmospheric Science Letters* 12: 13-18.

Marshall, S.F., Covert, D.S. and Charlson, R.J. (1995). Relationship between Asymmetry Parameter and Hemispheric Backscatter Ratio: Implications for Climate Forcing by Aerosols. *Applied optics* 34: 6306-6311.

Mathon, V. and Laurent, H. (2001). Life Cycle of Sahelian Mesoscale Convective Cloud Systems. *Quarterly Journal of the Royal Meteorological Society* 127: 377-406.

Myhre, G., D. Shindell, F.-M. Bréon, W. Collins, J. Fuglestvedt, J. Huang, D. Koch, J.-F. Lamarque, D. Lee, B. Mendoza, T. Nakajima, A. Robock, G. Stephens, T. Takemura and H. Zhan (2013). Anthropogenic and Natural Radiative Forcing. In: Climate Change 2013: The Physical Science Basis. Contribution of Working Group I to the Fifth Assessment Report of the Intergovernmental Panel on Climate Change [Stocker, T.F., D. Qin, G.-K. Plattner, M. Tignor, S.K. Allen, J. Boschung, A. Nauels, Y. Xia, V. Bex and P.M. Midgley (Eds.)], Cambridge University Press, Cambridge, United Kingdom and New York, NY, USA.

NOAA (1998). Automated Surface Observing System (Asos) Users' Guide, National Oceanic and Atmospheric Administration, USA.

Ogunjobi, K., He, Z. and Simmer, C. (2008). Spectral Aerosol Optical Properties from Aeronet Sun-Photometric Measurements over West Africa. *Atmospheric Research* 88: 89-107.

Pace, G., Sarra, A.d., Meloni, D., Piacentino, S. and Chamard, P. (2006). Aerosol Optical Properties at Lampedusa (Central Mediterranean). 1. Influence of Transport and Identification of Different Aerosol Types. *Atmospheric Chemistry and Physics* 6: 697-713.

Pani, S.K., Wang, S.-H., Lin, N.-H., Lee, C.-T., Tsay, S.-C., Holben, B.N., Janjai, S., Hsiao, T.-C., Chuang, M.-T. and Chantara, S. (2016). Radiative Effect of Springtime Biomass-Burning Aerosols over Northern Indochina During 7-Seas/Baseline 2013 Campaign. *Aerosol Air Qual. Res* 16: 2802-2817.

Ramachandran, S. and Kedia, S. (2010). Black Carbon Aerosols over an Urban Region: Radiative Forcing and Climate Impact. *Journal of Geophysical Research: Atmospheres* 115.

Rana, S., Kant, Y. and Dadhwal, V. (2009). Diurnal and Seasonal Variation of Spectral Properties of Aerosols over Dehradun, India. *Aerosol and Air Quality Research* 9: 32-49.

Reeves, C., Formenti, P., Afif, C., Ancellet, G., Attié, J.-L., Bechara, J., Borbon, A., Cairo, F., Coe, H. and Crumeyrolle, S. (2010). Chemical and Aerosol Characterisation of the Troposphere over West Africa During the Monsoon Period as Part of Amma. *Atmospheric Chemistry and Physics* 10: 7575-7601.

Rizzo, L.V., Artaxo, P., Muller, T., Wiedensohler, A., Paixao, M., Cirino, G.G., Arana, A., Swietlicki, E., Roldin, P., Fors, E., K. T. Wiedemann, Leal, L.S.M. and Kulmala, M. (2013). Long Term Measurements of Aerosol Optical Properties at a Primary Forest Site in Amazonia. *Atmospheric Chemistry and Physics* 13: 2391-2413.

Roberts, G., Wooster, M. and Lagoudakis, E. (2009). Annual and Diurnal African Biomass Burning Temporal Dynamics. *Biogeosciences* 6: 849-866.

Sheridan, P., Jefferson, A. and Ogren, J. (2002). Spatial Variability of Submicrometer Aerosol Radiative Properties over the Indian Ocean During Indoex. *Journal of Geophysical Research: Atmospheres* 107: INX2 10-11-INX12 10-17.

Sheridan, P.J. and Ogren, J.A. (1999). Observations of the Vertical and Regional Variability of Aerosol Optical Properties over Central and Eastern North America. *Journal of Geophysical Research: Atmospheres* 104: 16793-16805.

Stier, P., Feichter, J., Roeckner, E., Kloster, S. and Esch, M. (2006). The Evolution of the Global Aerosol System in a Transient Climate Simulation from 1860 to 2100. *Atmospheric Chemistry and Physics* 6: 3059-3076.

Sultan, B. and Janicot, S. (2000). Abrupt Shift of the Itcz over West Africa and Intra-Seasonal Variability. *Geophysical Research Letters* 27: 3353-3356.

Tiwari, S., Tiwari, S., Hopke, P., Attri, S., Soni, V. and Singh, A.K. (2016). Variability in Optical Properties of Atmospheric Aerosols and Their Frequency Distribution over a Mega City "New Delhi," India. *Environmental Science and Pollution Research* 23: 8781-8793.

Todd, M.C., Washington, R., Martins, J.V., Dubovik, O., Lizcano, G., M'bainayel, S. and Engelstaedter, S. (2007). Mineral Dust Emission from the Bodélé Depression, Northern Chad, During Bodex 2005. *Journal of Geophysical Research: Atmospheres* 112.

633 USEPA (2012). Report to Congress on Black Carbon. Epa-450/R-12-001, United States Environmental
634 Protection Agency, Research Triangle Park, NC.

635 Verma, S., Prakash, D., Srivastava, A.K. and Payra, S. (2017). Radiative Forcing Estimation of Aerosols at an
636 Urban Site near the Thar Desert Using Ground-Based Remote Sensing Measurements. *Aerosol and Air*
637 *Quality Research* 17: 1294-1304.

638 Virkkula, A., Levula, J., Pohja, T., Aalto, P., Keronen, P., Schobesberger, S., Clements, C.B., Pirjola, L.,
639 Kieloaho, A.-J. and Kulmala, L. (2014). Prescribed Burning of Logging Slash in the Boreal Forest of
640 Finland: Emissions and Effects on Meteorological Quantities and Soil Properties. *Atmospheric Chemistry*
641 *and Physics* 14: 4473-4502.

642 Wang, J., Xia, X., Wang, P. and Christopher, S.A. (2004). Diurnal Variability of Dust Aerosol Optical
643 Thickness and Angström Exponent over Dust Source Regions in China. *Geophysical Research Letters* 31.

644 Wiscombe, W. and Grams, G. (1976). The Backscattered Fraction in Two-Stream Approximations. *Journal of*
645 *the Atmospheric Sciences* 33: 2440-2451.

646 Yang, X., You, Z., Hiller, J. and Watkins, D. (2016). Updating and Augmenting Weather Data for Pavement
647 Mechanistic-Empirical Design Using Asos/Awos Database in Michigan. *International Journal of*
648 *Pavement Engineering*: doi: 10.1080/10298436.10292016.11234278.

649 Yoon, S.-C., Won, J.-G., Omar, A.H., Kim, S.-W. and Sohn, B.-J. (2005). Estimation of the Radiative Forcing
650 by Key Aerosol Types in Worldwide Locations Using a Column Model and Aeronet Data. *Atmospheric*
651 *Environment* 39: 6620-6630.
652